CIVIL ENGINEERING JOURNAL

Article no. 8

THE CIVIL ENGINEERING JOURNAL 1-2024

FINITE ELEMENT SIMULATION ANALYSIS OF CURVILINEAR CONTINUOUS BEAM BRIDGE JACKING AND TRANSLATION CONSTRUCTION

Xilong Zheng[1], Wei Li[1], Honglei Zhang[2] and Qiong Wang [1]

1. *School of Civil and Architectural Engineering, Harbin University, No.109 Zhongxing Road, Harbin, Heilongjiang Province, China; sampson88@126.com*
2. *Beijing xinqiao technology, No.8 Xitucheng Road, Haidian District, Beijing, China*

ABSTRACT

This paper investigates the issue of beam misalignment in curved continuous beam bridges. Taking the D0 to D6 spans of the Gongbin Road viaduct as the basis, the main influencing factors causing misalignment in curved beam bridges are analyzed and the causes of transverse and longitudinal misalignment in curved beam bridges are calculated and analyzed using Midas/Civil finite element simulation software. The results indicate that the main influencing factor causing misalignment in the operation of curved continuous beam bridges is the system temperature, with the displacement caused by it being larger than the cumulative displacement caused by self-weight, construction phase, gradient load, vehicle load, and bearing settlement. During operation, the failure of expansion joints changes the boundary conditions of the beam, preventing the bridge from freely expanding and contracting longitudinally under temperature load. As a result, the transverse displacement increases to 2-3 times the normal working state of the expansion joint, leading to beam misalignment.

KEYWORDS

Continuous beam bridge, Jacking simulation, Translation simulation, Misalignment, Simulation analysis

INTRODUCTION

Small and medium-span bridges account for approximately 88% of the total number of highway bridges in our country, and due to their large quantity, they deserve more attention in terms of daily maintenance and repair work [1-3]. Due to the fact that many of these bridges were built in the previous century, they were limited by the technology available at that time. As a result, their design load standards and capacity are inadequate to meet current requirements [4-7]. Currently, in China, the majority of funds allocated for highway bridge construction are focused on major bridge projects. As a result, there is limited funding available for small and medium-span bridges. For those smaller bridges that cannot meet current traffic demands, it is nearly impossible to demolish and reconstruct them on a large scale. Instead, it is necessary to modify these existing bridges, making them compliant with current traffic requirements [8-11].

To better renovate small and medium-span bridges and ensure their efficient service to the

people, it is crucial to address the common structural defects. However, there is still insufficient attention given to these issues. One such concern is the significant problem of lateral displacement in the superstructure, which severely affects the normal functioning of the bridges. In particular, small and medium-span curved continuous beam bridges are more prone to such displacements due to their complex structure and load characteristics under long-term effects [12]. Analyzing the causes of bridge lateral displacement is of great significance for improving the efficiency of treating this issue, reducing structural defects in small and medium-span bridges in China, and ensuring the safety of bridges during their operational phase [13-15]. This article will establish bridge models using finite element software to identify the influencing factors contributing to beam displacement. The objective is to analyze the extent to which these factors impact the lateral and longitudinal displacements of the bridge.

INTRODUCTION TO ENGINEERING BACKGROUND

The design load level for the elevated bridge is Class A. The main span of the Gongbin Road elevated bridge consists of 119 segments. This study mainly focuses on the displacement analysis of spans D0 to D6. The upper structure of spans D0 to D6 is a continuous curved box girder made of ordinary reinforced concrete, with a span combination of 20+4×25+20=140 m. The box girder is a twin-box six-cell structure with a height of 1.4 m. The total width of spans D0 to D6 is 28 m, and the width distribution is as follows: 0.5 m crash barrier + 12.0 m roadway + 2.0 m median strip + 12.0 m roadway + 0.5 m crash barrier. The lower structure consists of pier D1 to D5#, which are column-type bridge piers, and pier D6 is a prestressed concrete inverted T-shaped cap beam pier. The substructure also includes reinforced concrete rectangular abutments. The aerial view of the elevated structure is shown in Figure 1, and the elevation, plan, and cross-sectional views of the bridge are shown in Figure 2 - Figure 4.

Fig. 1 – Aerial view of the elevated bridge

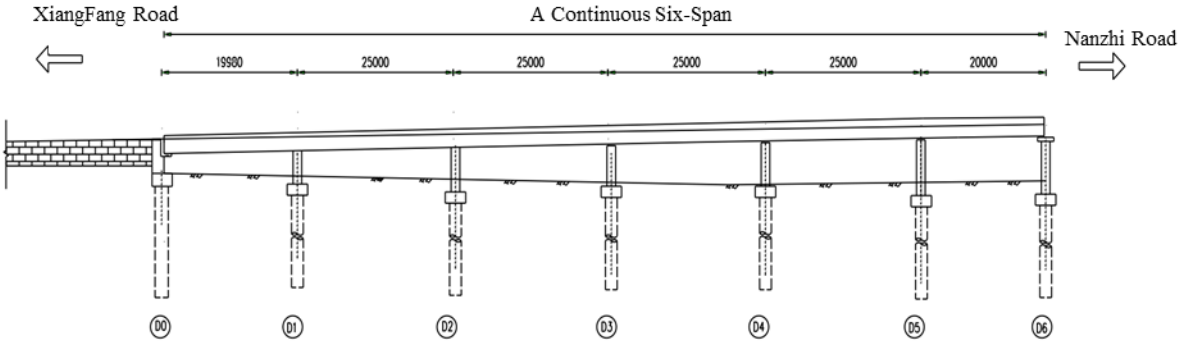

Fig. 2 – Bridge elevation layout diagram (unite: mm)

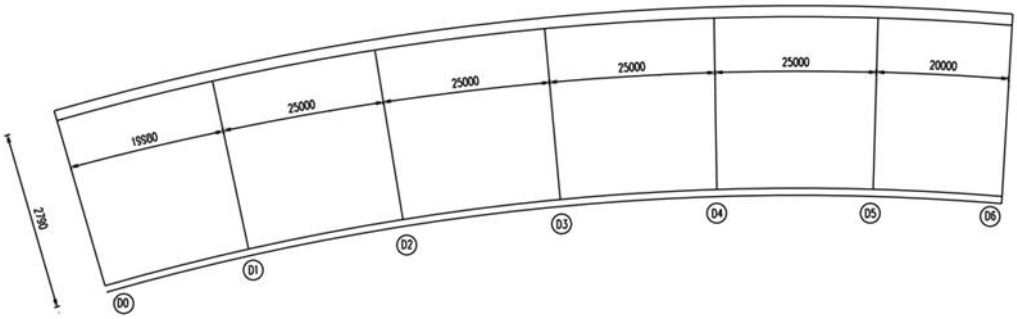

Fig. 3 – Plan layout diagram (unite: mm)

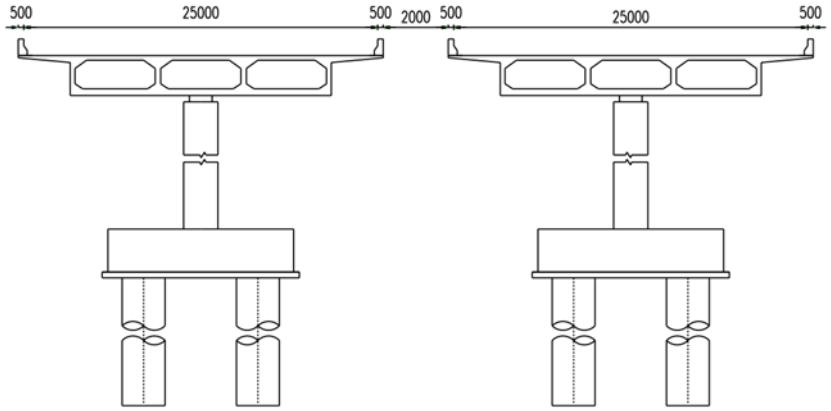

Fig. 4 – Cross-section layout diagram (unite: mm)

OFFSETTING DEFECT

(1) During the inspection of a curved continuous beam bridge, significant lateral displacement of the main beam towards the outside of the curve was observed. The D6# pier box beam exhibited the most noticeable lateral displacement, with a measured lateral displacement at the end of the continuous box beam of at least 90 mm at the outer side of the curve abutment. Due to this lateral displacement, the continuous box beam has caused severe structural damage to its lower bearings, the bridge piers, and even the adjacent ramp bridge. At the end of the 6# pier cap beam (outer side of the curved beam), the retaining block has fractured under the lateral pressure exerted by the main beam, posing a risk of falling as shown in Figure 5.

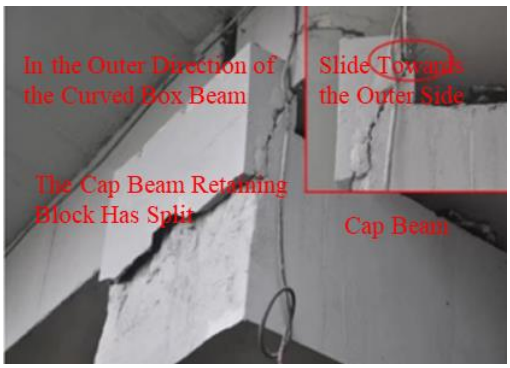

Fig. 5 – Diagonal splitting of bridge abutment cap beam block

(2) The lateral displacement of the curved girder bridge will cause the steel plate on the bearing to move along with it. Inspection revealed that there is a common phenomenon of outward sliding movement of the upper steel plate in the bidirectional movable bearings, and in some severe cases, there is a 40 mm displacement between the upper steel plate and the steel basin, as shown in Figure 6 and Figure 7.

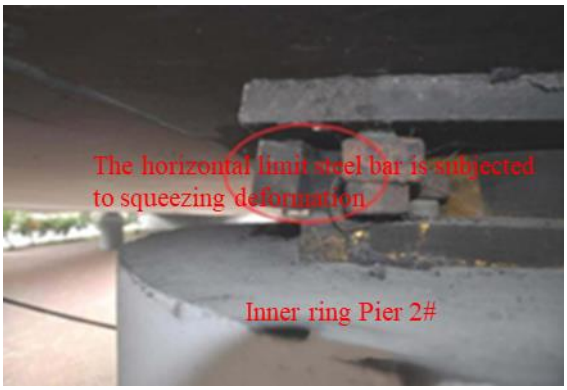

Fig. 6 – Compression deformation of lateral restraining steel bar

Fig. 7 – Sliding of upper steel plate out of steel basin by 40 mm

(3) The lower outer surface of the bridge pier column has several semi-circular cracks, as shown in Figure 8. The maximum width of the cracks is 0.26 mm. The crack distribution schematic is shown in Figure 9. The analysis indicates that this is due to the presence of fixed basin-type bearings above the bridge pier. The lateral displacement tendency of the main beam is constrained by the fixed bearings. According to the principle of force interaction, the main beam exerts radial forces on the bearings in the crawling direction, causing a transition of the bridge pier column from an axially compressed state to an eccentrically compressed state and even resulting in tensile stress in the outer concrete.

Fig. 8 – Bottom half-ring crack in bridge pier concrete

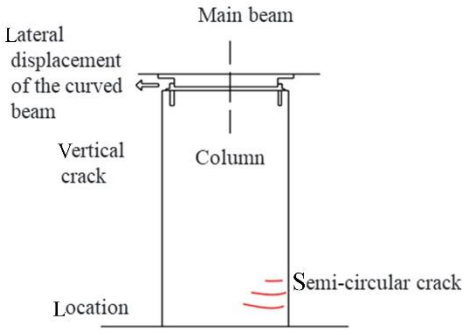

Fig. 9 – Schematic diagram of crack in bridge pier column

MODEL ESTABLISHMENT

The process of bridge jacking and translation may appear simple, but the selection of construction schemes and the control standards during construction are extremely complex. The main challenge lies in how to control the displacement and stress of the beam within a reasonable range during the construction process, without causing damage to the beam. To address this issue,

a focused analysis is conducted on the causes of beam deformation and stress during construction, in order to identify corresponding avoidance measures.

Simulation of the Boundary for Curve Continuous Beam Jacking

(1) Selection of jacking method. Bridge jacking techniques can be divided into two categories: integral jacking and partial jacking. Due to the fact that the D0~D6 spans of the Gongbin Elevated Bridge consist of a six-span continuous beam structure, and considering the relatively large jacking height required for this project, the integral jacking method is adopted to minimize damage to the beam. The jacking process mainly includes installing temporary supports, jacking the beams, replacing bearings, and releasing the oil from the jacks, totally four phases. The specific operational steps are illustrated in Figure 10.

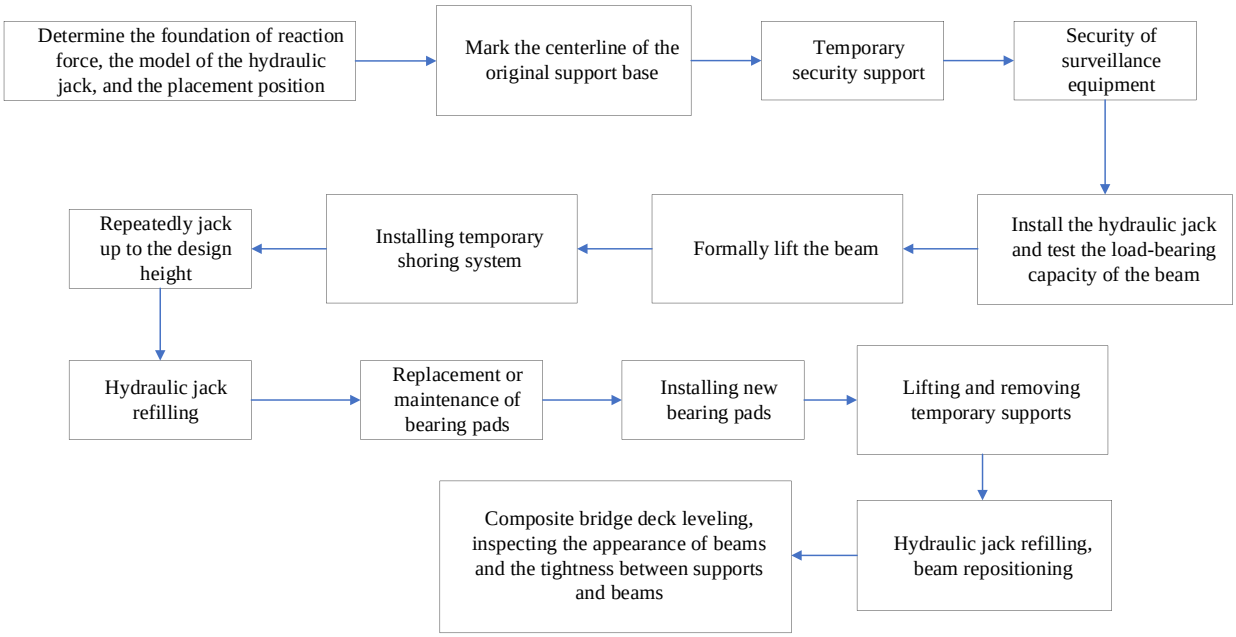

Fig. 10 – Jacking construction steps

(2) In the process of synchronously jacking a bridge, the main control is the variation of the beam stress values generated by the height difference during the start of synchronous jacking and the final placement of the beam. Therefore, the simulation of the supports is controlled by node displacement to achieve the desired effect.

(3) The main beam supports of the original bridge design adopt the form of GPZ8000 pot rubber bearings. Therefore, this paper simulates the bridge supports using compressed springs.

(4) Bridge uplift force and lifting height design.

Based on the size of the beam and considering the effects of various adverse loads, the rated lifting force of the jack is increased by 200% as a safety margin. When lifting the bridge, a 650t hydraulic jack with mechanical locks is used, and the lifting height is 80 mm. The method of staged synchronous lifting is adopted.

Simulation of The Translation Boundary of a Curved Continuous Beam Bridge.

(1) The bridge displacement construction method adopts the whole top pushing and resetting construction method.

(2) During the vertical boundary simulation of bridge displacement and resetting construction, the bowl-shaped rubber bearings have been removed. Horizontal sliding devices are used as vertical supports for the beam structure during the displacement construction. Polyethylene PTFE sheets are applied with silicone oil to reduce friction during construction. Therefore, during the simulated process of top pushing and displacement, compressed rigid supports are used to replace the vertical boundary conditions of the main beam.

(3) During the lateral boundary simulation of bridge displacement and resetting, the lateral boundary conditions of the beam are released. Under the thrust of the jacks, the beam overcomes the frictional resistance of the slide and moves towards the inner side of the arc. During the displacement process, the beam mainly undergoes rigid body motion; at the same time, the beam may experience small recoverable deformations. When the beam is translated to the contact with the stopper at the end of the beam and the bridge abutment, the stopper acts as a lateral rigid constraint. The beam will cease rigid body rotation and accompanied by significant recoverable deformations.

(4) The design of lateral top pushing force and displacement for the bridge. When the main beam is laterally pushed, considering the adverse factors such as temperature stress and the shear deformation of the bearings themselves, the principle of adding a 200% safety margin to the rated lifting force of the jacks is followed. For the displacement process, a 150 T jack is selected for controlled top pushing with graded control. The top pushing speed of the jacks during horizontal displacement should not exceed 1mm/min to ensure that the entire beam moves towards the inner side of the curve as per design requirements.

Control of The Uplift and Translation Reaction Forces.

During the uplift and translation resetting operation of the bridge under traffic closure, it is crucial to ensure that there is no void under the bearings. This means that the bridge, in its displaced state, must have a minimum reaction force of the jacks that is not less than 0 under the most unfavorable load combinations, controlled by hydraulic pressure. This is necessary to prevent the risk of beam overturning and to perform stress verification.

The finite element model is established by using the finite element software Midas/Civil. The main beam is simulated by the beam element and the support is generally supported. During the lifting process, forced displacement is applied to the position of the support. One fixed support is on the D3 pier, and the rest are movable supports.

In the condition of traffic closure, the minimum reaction forces of each bearing of the bridge under the load combination of 1.2 dead load + 1.4 live load are shown in Figure 11.

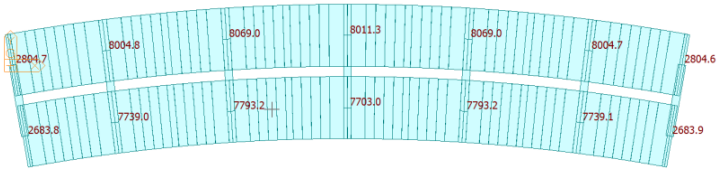

Fig. 11 – Bearing reaction forces

When the bridge reaches its maximum displacement of 90 mm under traffic closure, the minimum value of the inner-side bearing reaction force for a curved girder bridge is 2683.9 kN, and

the support force of the jacks is greater than 0. Therefore, it can be concluded that when the beam displacement reaches 90 mm under traffic closure, the bridge support is in a safe condition.

In the condition where traffic is not controlled and vehicles travel along the original lanes, the reaction forces at each support position are shown in Figure 12. In this state, the minimum bearing reaction force is 2432.5 kN. Hence, it can be concluded that when the bridge is in a displaced condition without traffic control, the support forces decrease under the action of eccentric loads. If the bridge is not properly maintained and continues to operate in the displaced state, the displacement will continue to increase, and there is a risk of overturning under the action of eccentric loads.

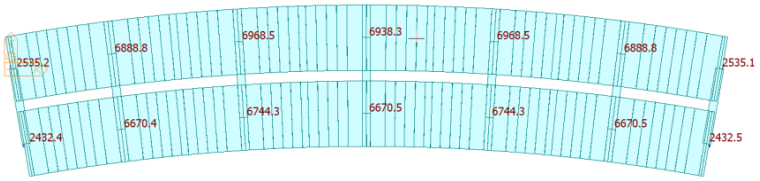

Fig. 12 – Bearing reaction forces

Hydraulic Lifting Stress Control

Traffic control is required during the construction of hydraulic lifting and translation to ensure construction safety and normal travel for the public. The stress increment generated at the most critical section during the construction process should be less than the stress increment generated by live loads at the same section.

Under the action of the most unfavourable eccentric load, tensile stress is generated at the upper edge of the main beam section as Pt, and compressive stress is generated in the main beam section as Pc. To ensure the safety and sufficient safety factor of the main beam during the hydraulic lifting and translation construction process, the stress variation at the most critical section is controlled to not exceed 80% of the stress increment under the action of live loads at the same section. Specifically, the incremental tensile stress at the most critical section of the main beam should not exceed 0.8 Pt, and the incremental compressive stress at the most critical section of the main beam should not exceed 0.8 Pc, which ensures the safety of the construction. The calculation results are shown in Figure 13.

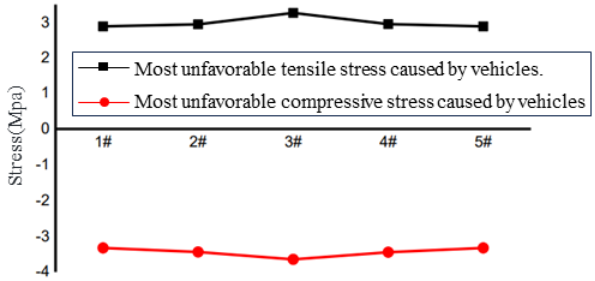

Fig. 13 – The stress limits during the bridge translocation and repositioning process

Using this stress control method is safer and more accurate compared to directly using the design value of concrete tensile strength as the construction stress control criteria.

SIMULATION ANALYSIS OF CURVED CONTINUOUS BEAM BRIDGE.

Simulation of the Jacking Process

In the jacking process of the bridge, a step-by-step jacking method is adopted, with a jacking increment of 5-10 mm per step. This study takes a step increment of 10 mm as an example to analyze the stress increment of each section under different jacking conditions. The specific conditions are listed in Table 1.

Tab. 1 - Simulation of Jacking Conditions

Operating condition	The jacking height
Operating condition one	10 mm single-point jacking for Pier 0 and Pier 3
Operating condition two	Pier 0 jacked up by 10 mm, Pier 1 jacked up by 5 mm, Pier 3 jacked up by 10 mm, Pier 2 and Pier 4 jacked up by 5 mm
Operating condition three	Pier 0 jacked up by 10 mm, Pier 1 jacked up by 8 mm.Pier 3 jacked up by 10 mm, Pier 2 and Pier 4 jacked up by 8 mm
Operating condition four	Synchronized jacking up by 10 mm

(1) Condition 1: The single-point jacking of Piers 0 and 3 by 10 mm. The increment of stress and deformation of the main beam is shown in Figure 14 – Figure 17.

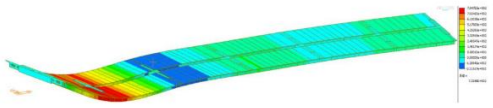

Fig. 14 – Stress distribution diagram of main beam (0# Abutment raised by 10 mm)

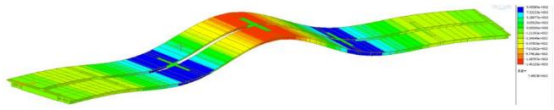

Fig. 15 – Stress distribution diagram of main beam (3# Pier cap raised by 10 mm)

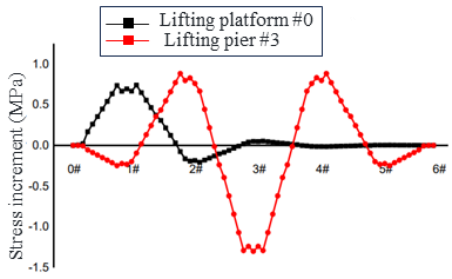

Fig. 16 – Increment of stress on the lower edge of the main beam during single point jacking

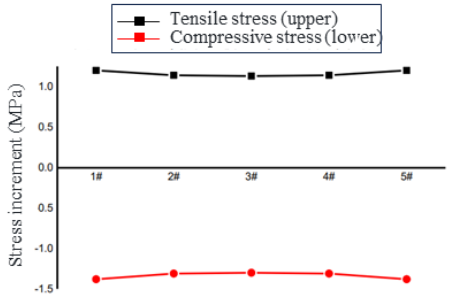

Fig. 17 – Increment of stress on main beam cross-sections for each pier during single point jacking

From the above figure, when the single point is raised to 10 mm, the main beam section at the 0# abutment is in an unconstrained state, resulting in no increase in the bottom stress increment. However, the adjacent main beam section at the 1# pier has a positive increase in bottom stress, indicating tensile stress, and the maximum stress value. When the single point is raised to 10 mm at the 3# pier, the bottom stress increment at the 3# pier is negative, indicating compressive stress and the maximum stress value, while the bottom stress increment at the adjacent piers 2# and 4# is positive, indicating tensile stress with relatively large stress values.

(2) Condition 2: The lifting height at the 0# abutment and the 3# pier is 10 mm, while the adjacent piers on the left and right have a lifting height of 5 mm. The stress increments and deformations of the main beam section are shown in Figure 18 - Figure 21.

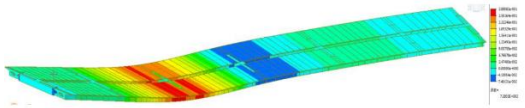

Fig. 18 – Stress distribution diagram of main beam (0# Abutment raised)

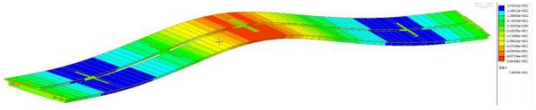

Fig. 19 – Overall bridge stress distribution diagram (3# Pier raised)

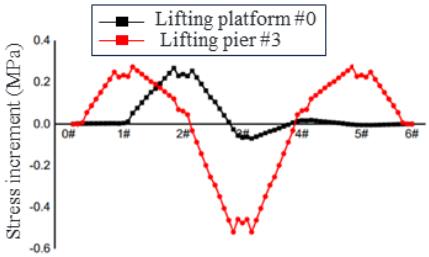

Fig. 20 – Increment of stress on the lower edge of the main beam (0# Abutment, 3# Pier raised)

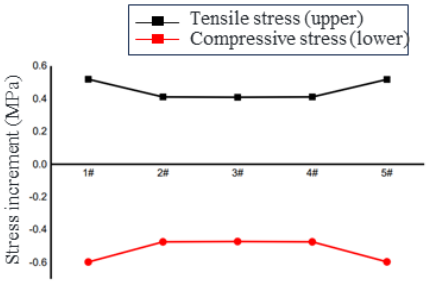

Fig. 21 – Maximum increment of stress on the main beam (1#~5# Pier raised)

From the above figures, it can be observed that when the 0# abutment is lifted to 10 mm and the 1# pier is lifted to 5 mm, the main beam section at the 0# abutment experiences no increase in bottom stress increment due to its unconstrained state. However, the bottom stress increment at the adjacent 1# and 2# piers undergo significant changes. When the 3# pier is lifted to 10 mm and both the 2# and 4# piers are simultaneously lifted to 5 mm, the stress increment across the entire bridge remains large.

(3) Condition 3: The lifting height at the 0# abutment and the 3# pier is 10 mm, while the adjacent piers on the left and right have a lifting height of 8 mm. The stress increments and deformations of the main beam section are shown in Figure 22 - Figure 25.

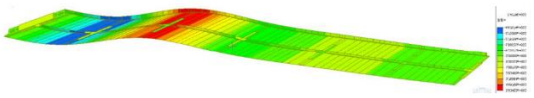

Fig. 22 – Stress distribution diagram of the main beam (0# Abutment raised)

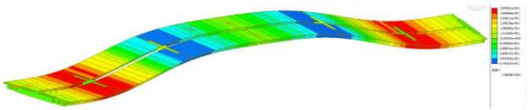

Fig. 23 – Stress distribution diagram of the main beam (3# Pier raised)

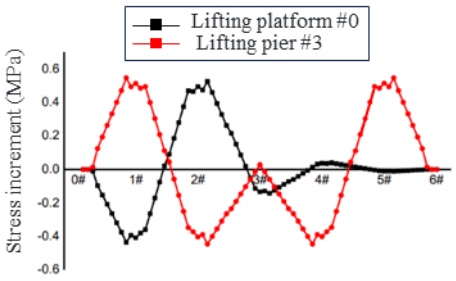

Fig. 24 – Increment of stress on the lower edge of the main beam (0# Abutment, 3# Pier raised)

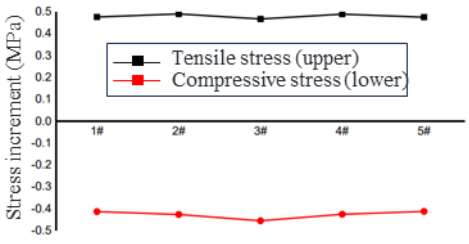

Fig. 25 – Maximum increment of stress on the main beam (1#~5# Pier raised)

From the above figures, it can be seen that when the 0# abutment is lifted to 10 mm and the 1# pier is lifted to 8 mm, the stress increments across the entire bridge are not significant. However, when the 3# pier is lifted to 10 mm and both the 2# and 4# piers are simultaneously lifted to 8 mm, the stress increment at the 3# pier is relatively large and compressive, while the stress increments at the other piers and abutments are relatively small.

(4) Condition 4: Synchronized lifting of the entire bridge by 10 mm, the stress increments of the main beam section are shown in Figure 26.

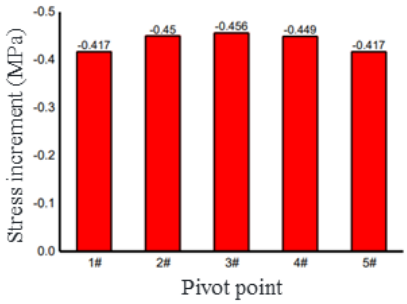

Fig. 26 – Increment of stress on the lower edge of the main beam during synchronized lifting

From the above figure, it can be observed that when the entire bridge is synchronously lifted by 10 mm, the stress increments at the 1# to 5# piers are relatively uniform and the magnitude of the stress increments is also similar.

By utilizing finite element software, a simulation analysis was conducted to analyze the stress increments of the entire bridge under four different loading conditions when the incremental lifting height reached 10 mm. Due to the significantly large total weight and a lifting height of 80 mm for the Gongbin Road viaduct, considering its structural system as a continuous beam bridge, the synchronized lifting scheme is deemed more reasonable, resulting in relatively minimal structural damage.

SIMULATION ANALYSIS OF THE TRANSLATIONAL PROCESS

The translational process simulation is carried out by simulating the top pushing force through the application of concentrated forces. Multiple loading conditions are simulated based on different directions and magnitudes of the top pushing force. The details are as follows.

(1) Condition 1: During the translational process, the jacks exert equal pushing forces in a direction perpendicular to the beam end, pushing towards the inside of the curve. The angle between the pushing force direction and the tangent line of the curve is shown in Table. 2. When simulating the pushing force direction of the bridge using finite element software, the angle between the pushing force direction and the Y-axis is shown in Table 3. The displacement in the transverse, longitudinal, and vertical directions of the main beam is shown in Figure 27 - Figure 29. The maximum stress increments on the upper and lower edges, as well as the inner and outer sides of the main beam, are shown in Figure 30 - Figure 33.

Tab. 2 - Angle between the top-down direction at various support point locations and the normal of the curve

Pivot point	Platform#0	Pier #1	Pier #2	Pier #3	Pier #4	Pier #5	Pier #6
Angle (°)	-9.96	-7.16	-3.58	0	3.58	7.16	9.96

Table. 3 - Angle between the top-down direction and the Y-axis at various support point locations

Pivot point	Platform#0	Pier #1	Pier #2	Pier #3		Pier #4	Pier #5	Pier #6
Angle (°)	0	0	0	0		0	0	0

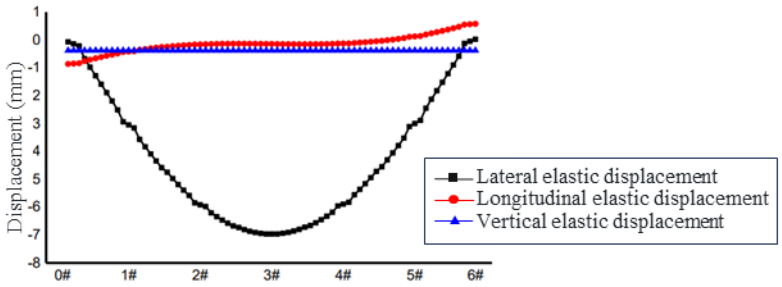

Fig. 27 – Three-dimensional elastic displacement of the main beam during translation process

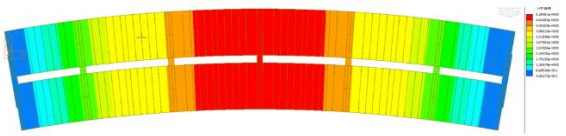

Fig. 28 – Deformation diagram of the main beam during translation process

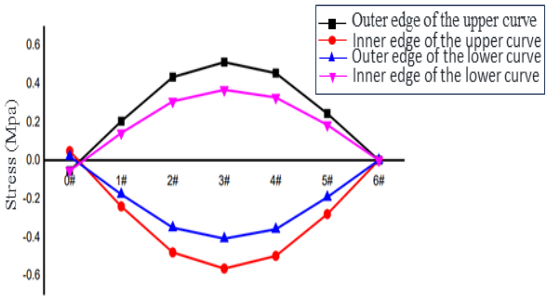

Fig. 29 – Stresses on upper and lower flanges, inner and outer sides of the main beam during translation process

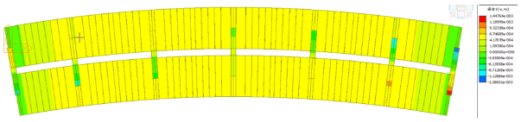

Fig. 30 – Stress distribution on the upper outer surface of the main beam section during translation process

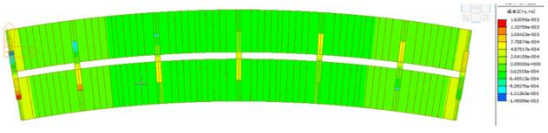

Fig. 31 – Stress distribution on the upper inner surface of the main beam section during translation process

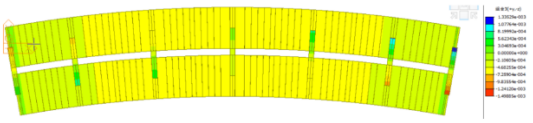

Fig. 32 – Stress distribution on the lower outer surface of the main beam section during translation process

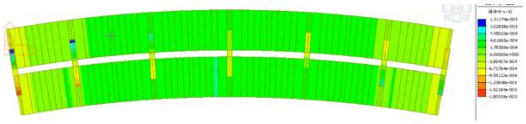

Fig. 33 – Stress distribution on the lower inner surface of the main beam section during translation process

(2) Condition 2: The pushing force is applied in the direction perpendicular to the main beam's line form, pushing towards the inside of the curve. The pushing force magnitude is the same for each pier section. The angle between the pushing force direction and the curve's normal vector is shown in Table 4. When simulating the pushing force direction of the bridge using finite element software, the angle between the pushing force direction and the Y-axis is shown in Table 5.

Tab. 4 - Angle between thrust direction and curve normal at various support locations

Pivot point	Platform#0	Pier #1	Pier #2	Pier #3	Pier #4	Pier #5	Pier #6
Angle (°)	0	0	0	0	0	0	0

Tab. 5 - Angle between thrust direction and Y-axis at various support locations

Pivot point	Platform#0	Pier #1	Pier #2	Pier #3	Pier #4	Pier #5	Pier #6
Angle (°)	9.96	7.16	3.58	0	-3.58	-7.16	-9.96

The maximum deformation in the transverse, longitudinal, and vertical directions of the main beam is shown in Figure 34. The stress deformation cloud diagram of the main beam during translation is shown in Figure 35. The maximum stress increments on the upper and lower edges, as well as the inner and outer sides of the main beam, are shown in Figure 36.

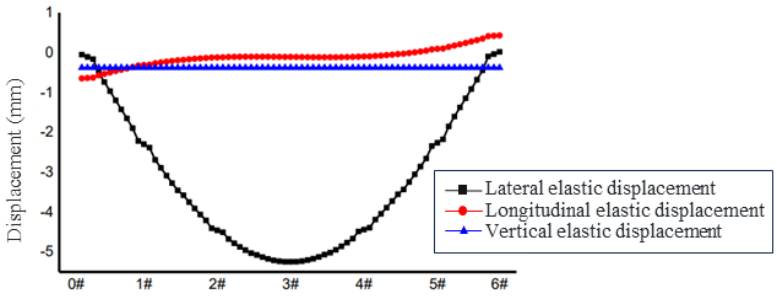

Fig. 34 – Three-dimensional elastic displacement of the main beam during translation process

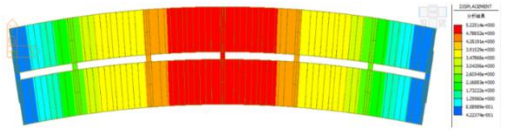

Fig. 35 – Deformation diagram of the translated main beam

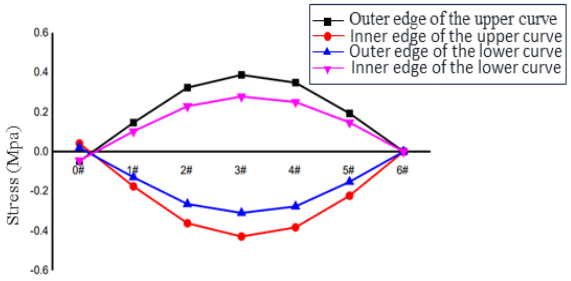

Fig. 36 – Stresses on the upper and lower flanges, inner and outer sides of the translated main beam

(3) Condition 3: The pushing force direction is along the line perpendicular to the beam end and pushing towards the inside of the curve. The maximum deformations in the transverse, longitudinal, and vertical directions of the main beam are shown in Figure 37. The stress deformation cloud diagram of the main beam during translation is shown in Figure 38. The maximum stress increments on the upper and lower edges, as well as the inner and outer sides of the main beam, are shown in Figure 39.

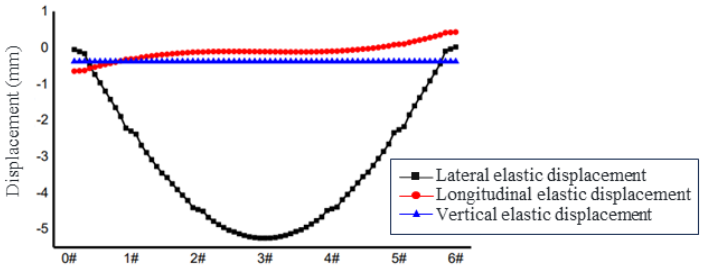

Fig. 37 – Three-dimensional elastic displacement of the main beam during translation process

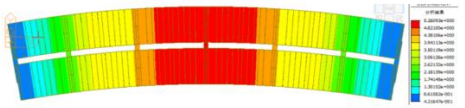

Fig. 38 – Deformation diagram of the translated main beam

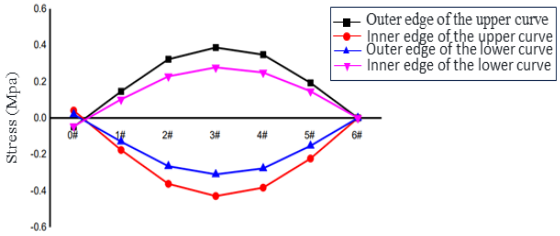

Fig. 39 – Stresses on the upper and lower flanges, inner and outer sides of the translated main beam

Condition 3, when compared to Conditions 1 and 2, exhibits smaller stresses and elastic deformations during construction, ensuring the safety of the beam structure. However, controlling the pushing force of the jacks during the pushing operation in Condition 3 can be challenging. If not finely controlled, there is a possibility that the pushing force may not overcome the frictional resistance, resulting in the inability of the beam to rotate.

Condition 2, in comparison to Condition 1, offers superior stress and deformation characteristics.

With the project located on a curved surface with a radius of curvature of 400 m, when pushing forces are applied perpendicular to the beam's end line, significant horizontal bending deformations of the main beam will occur during the pushing process, and the radius of curvature will decrease.

CONCLUSION

Discussion on the rigid body state of the bridge during the lifting, translation, and resetting construction process, deriving a reasonable method for bridge lifting and translation construction, as well as establishing a model. Proposing stress limitation criteria during the lifting and translation process. Then, based on the aforementioned model establishment method, a finite element model of the actual bridge is established, and a simulation analysis is conducted on the lifting and translation process of the project. The following conclusions are reached:

(1) Under various load conditions, temperature load (specifically system load) has a significant impact on the deflection of curved beam bridges. Its influence is even greater than the cumulative displacement caused by self-weight, construction phase load, gradient load, vehicle load, and bearing settlement, highlighting its importance. In China, there is a significant temperature difference between the north and south. In the southern regions, it is necessary to consider the overall temperature rise and its effects on the deflection of curved beam bridges, while in the colder northern regions, greater consideration should be given to the overall temperature decrease and its effects on the deflection of curved beam bridges.

(2) The closer the lifting height of the main beam at the pier and bridge abutment, the more similar the growth pattern of the section stress values. When synchronous lifting was employed, the stress values were all within 0.45 MPa and below the ultimate stress limit. Due to the large lifting height required for the project, it is necessary to control the stress differences. Therefore, the synchronous lifting construction method was adopted.

(3) During the translation construction phase of the beam, a concentrated force was applied to simulate the pushing force of a hydraulic jack. Combining with the model, the movement form and stress state of the beam under different pushing force directions and magnitudes during the translation process were discussed. Safety in construction and the difficulty of construction control were taken into consideration to derive a reasonable construction plan.

REFERENCE

[1] Zhai, Zhihao, Chengbiao Cai, and Shengyang Zhu. Implementation of Timoshenko curved beam into train-track-bridge dynamics modelling[J]. International Journal of Mechanical Sciences, 2023, 247: 108158.

[2] Linzell, D. G., and J. F. Shura. Erection behavior and grillage model accuracy for a large radius curved bridge[J]. Journal of Constructional Steel Research, 2010, 66(3): 342-350.

[3] Li, Ming, and Jingqiao Hu. Analysis of heterogeneous structures of non-separated scales using curved bridge nodes[J]. Computer Methods in Applied Mechanics and Engineering, 2022, 392: 114582.

[4] Tondini, Nicola, and Bozidar Stojadinovic. Probabilistic seismic demand model for curved reinforced concrete bridges[J]. Bulletin of earthquake engineering, 2012, 10: 1455-1479.

[5] Dimitrakopoulos, Elias G., and Qing Zeng. three-dimensional dynamic analysis scheme for the interaction between trains and curved railway bridges[J]. Computers & Structures, 2015, 149: 43-60.

[6] Wang, Jianwei, et al. Application of High-Viscosity Modified Asphalt Mixture in Curved Bridge Pavement[J]. Sustainability, 2023, 15(4): 3411.

[7] Seo, Junwon, and Daniel G. Linzell. Use of response surface metamodels to generate system level fragilities for existing curved steel bridges[J]. Engineering Structures, 2013, 52: 642-653.

[8] Kim, Woo Seok, Jeffrey A. Laman, and Daniel G. Linzell. Live load radial moment distribution for horizontally curved bridges[J]. Journal of Bridge Engineering, 2007, 12(6): 727-736.
[9] Zeng, Qing, Y. B. Yang, and Elias G. Dimitrakopoulos. Dynamic response of high speed vehicles and sustaining curved bridges under conditions of resonance[J]. Engineering Structures, 2016, 114: 61-74.
[10] Monzon, Eric V., Ian G. Buckle, and Ahmad M. Itani. Seismic performance and response of seismically isolated curved steel I-girder bridge[J]. Journal of Structural Engineering, 2016, 142 (12): 04016121.
[11] DeSantiago, Eduardo, Jamshid Mohammadi, and Hamadallah MO Albaijat. Analysis of horizontally curved bridges using simple finite-element models[J]. Practice Periodical on Structural Design and Construction, 2005, 10(1): 18-21.
[12] Ni, Yongjun, et al. Influence of earthquake input angle on seismic response of curved girder bridge[J]. Journal of traffic and transportation engineering (English edition), 2015, 2(4): 233-241.
[13] Wen, Q., et al. Control of human-induced vibrations of a curved cable-stayed bridge: Design, implementation, and field validation[J]. Journal of Bridge Engineering, 2016, 21(7): 04016028.
[14] Nevling, D., Daniel Linzell, and J. Laman. Examination of level of analysis accuracy for curved I-girder bridges through comparisons to field data[J]. Journal of Bridge Engineering, 2016, 11(2): 160-168.
[15] Zhang, Lixin, and Yin Gu. Seismic analysis of a curved bridge considering soil-structure interactions based on a separated foundation model[J]. Applied Sciences, 2020,10(12) :4260.